A Comparative Analysis of Different Turbulence Models for Simulating Complex Turbulent Separated Flows over Cubic Geometries

A Comparative Analysis of Different Turbulence Models for Simulating Complex Turbulent Separated Flows over Cubic Geometries

Nurgeldy Praliyev[1], Aydarkhan Sarsen[1], Nazira Kaishubayeva[1], Yong Zhao[1,*], Sai Cheong Fok[1] and Soo Lee Teh[1]

[1]Department of Mechanical and Aerospace Engineering, Nazarbayev University, Astana, Kazakhstan, 010000

[*]Corresponding author's E-mail: yong.zhao@nu.edu.kz

Abstract. This study is aimed to compare the performance of four Reynolds Averaged Navier Stokes (RANS) turbulence models in simulating complex flow over two- and three-dimensional (2D and 3D) cubic geometries using experimental measurements for model validation. The four turbulence models were k-Epsilon (k- ε), k-Omega (k- ω), Shear Stress Transport (SST) and BSL Reynolds Stress (RSM) models. The model validation was performed by comparative analysis with the experimental values of pressure coefficient around the cubic geometries. It was found that the SST and BSL RSM models performed better than the others in capturing the complex separated flows and strong shear in the boundary layer. The good agreement with empirical data can be attributed to the inclusion of transport effects of turbulence and the anisotropic nature in the formulations of the models.

1. Introduction

The fluid flow around bluff bodies is of great interest in engineering. Computational Fluid Dynamics (CFD) has become a useful tool in the study of wind around buildings and for the improvement of building design [1, 2, 3]. Poor wind engineering analysis of buildings may lead to issues during their construction and operation. For instance, in 2018, quite a few buildings in Astana (Kazakhstan) were damaged because of strong wind gusts, which reached the speed of 25 m/s. Later it was found that these building structures did not match local authority construction standards, according to which the environmental conditions of the local area must be considered [4]. Therefore, it is important to test buildings design under different environmental conditions (including strong wind, heavy rain etc.) using engineering tools, such as CFD, especially for areas such as Astana, where average wind speed exceeds 14 m/s, and occasionally reaches 23 m/s [5, 6]. According to the statistical study by Koppen [7], the majority of buildings in Astana are of rectangular and cube shapes. For this reason, it was decided in this study to investigate turbulent flow over a cubic block using different turbulence models, namely, Shear Stress Transport (SST), k-Epsilon (k-ε), k-Omega (k-ω) and BSL Reynolds Stress Model (RSM). The models were chosen since turbulent flow over a bluff body such as a cube has massive flow separation zones, which are difficult to predict accurately with the Reynolds-Averaged Navier-Stokes (RANS) turbulence simulation. In addition, the study of flow characteristics around bluff bodies such as cubes is always a significant topic in academic research as well as in engineering applications [8].

There are a number of studies on flow around cubes, though they are limited to experimental analysis. Certain flow parameters including static pressure coefficient have been measured over the cube surfaces in those empirical studies. One of the mostly cited paper in this area is the study of turbulent boundary layer flow over a cube by Castro et al. [9], who measured surface pressure coefficient of the cube at different Reynolds numbers. Authors concluded that the effects of Reynolds number (Re) existed for smooth laminar upstream flow, whereas for fully developed turbulent boundary layer the effect disappeared. Furthermore, no effects of Reynolds number have been found when Reynolds Number was greater than 4000.

Regarding the comparison of large eddy simulation for two- and three-dimensional computations for two-dimensional geometry, few papers have shown numerical results for the static pressure coefficient and compared it with that of the three-dimensional analysis for the same geometry. However, there is still doubt whether two-dimensional analysis is adequately representative of the flow in reality to replace three-dimensional analysis in order to avoid expensive three-dimensional computations and measurements. Murakami and Mochida [10] analysed unsteady flow over a two-dimensional square cylinder and compared the results of both 2D and 3D computations. Numerical results for 2D cube showed several discrepancies in comparison with those of 3D cube. Several researchers attributed the deviations to different boundary conditions (where 3D models allow for more realistic BCs), different meshing and boundary-layer development of turbulent flow. Nevertheless, it was noticed that differences in results can be significantly reduced by employing proper turbulent models. They concluded that the standard k-ε model fails in reproducing the vortex shedding, while the BLS RSM could do so rather well in comparison with other models.

Experimental findings by Lee, Y. T et al. [11] have been used by many researchers for validation of turbulence models for air flow over rectangular buildings with various aspect ratios and wind directions. It was found that the k-epsilon model results are in overall agreement with the experimental findings, but sometimes it does not capture certain flow features, for instance, in the regions close to the leading edge. In addition, the surface pressure variation is highly dependent upon the approaching wind direction, and the pressure coefficient is different at various positions on the top face of the three-dimensional rectangular geometry.

Most flows are three-dimensional, turbulent and transient, but it is very computationally expensive to conduct numerical studies on three-dimensional cases with the most realistic conditions. For that reason, the majority of previous studies were limited to two-dimensions [12]. For the current work, however, it was decided to conduct numerical analysis on both two- and three-dimensional cube geometries and make a brief comparison study. The main aim of the work was to compare four turbulence models, namely SST, k-ε, k-ω, BSL RSM and to identify the most accurate one based on its prediction of the flow around the cube both in 2D and 3D. The simulations were based on the experimental setup of Lee, Y. T et al. [10], in which a cube of 80x80x80 mm was tested in the wind tunnel of 320(h) x 560(w) x 1120(l) mm. More detailed information regarding the experimental setup and dimensions is given in the main body.

The current paper is divided into the following sections. First, the governing equations are discussed in the second section. Then, boundary and initial conditions of the numerical computation are presented in the third section. The fourth section covers information on the computational domain and the mesh verification study. Validation of the model and numerical results for the selected turbulence models are presented in the fifth section. The concluding remarks of the key findings are given in the final section.

2. Governing equations

The governing equations were derived based on the following assumptions: the air flow under study is statistically steady, incompressible and turbulent, for which the Reynolds-Averaged Navier-Stokes (RANS) equations are given below:

$$\frac{\partial}{\partial x_i}(\rho u_i) = 0 \tag{1}$$

$$\frac{\partial}{\partial x_j}\left(\rho u_i u_j\right) = -\frac{\partial p}{\partial x_i} + \frac{\partial}{\partial x_j}\left(\tau_{ij} + {\tau_{ij}}^R\right) + S_i\,;\;\; i = 1{,}2 \tag{2}$$

with

$$\tau_{ij} = \mu\left(\frac{\partial u_i}{\partial x_j} + \frac{\partial u_j}{\partial x_i} - \frac{2}{3}\sigma_{ij}\frac{\partial u_k}{\partial x_k}\right) \tag{3}$$

The Boussinesq turbulent eddy viscosity model was employed for the two-equation turbulence models:

$${\tau_{ij}}^R = \mu_t\left(\frac{\partial u_i}{\partial x_j} + \frac{\partial u_j}{\partial x_i} - \frac{2}{3}\sigma_{ij}\frac{\partial u_k}{\partial x_k}\right) - \frac{2}{3}\rho k\delta_{ij} \tag{4}$$

k-ε equations

The Turbulence Kinetic Energy Equation is as follows:

$$\frac{\partial}{\partial x_i}(\rho u_i k) = \frac{\partial}{\partial x_i}\left(\left(\mu + \frac{\mu_t}{\sigma_k}\right)\frac{\partial k}{\partial x_i}\right) + S_k \tag{5}$$

The Specific Dissipation Rate Equation is given below:

$$\frac{\partial}{\partial x_i}(\rho u_i \varepsilon) = \frac{\partial}{\partial x_i}\left(\left(\mu + \frac{\mu_t}{\sigma_\varepsilon}\right)\frac{\partial e}{\partial x_i}\right) + S_e \tag{6}$$

where, the source terms were defined as

$$S_k = {\tau_{ij}}^R\frac{\partial u_i}{\partial x_j} - \rho\varepsilon + \mu_t P_B \tag{7}$$

$$S_\varepsilon = C_{\varepsilon 1}\frac{\varepsilon}{k}\left(f_1{\tau_{ij}}^R\frac{\partial u_i}{\partial x_j} + \mu_i C_B P_B\right) - C_{\varepsilon 2}f_2\frac{\rho\varepsilon^2}{k} \tag{8}$$

$$P_B = -\frac{g_i}{\sigma_B}\frac{1}{\rho}\frac{\partial \rho}{\partial x_i} \tag{9}$$

with $g_i = (g_x, g_y)$ the gravity vector, the constant σ_B=0.9 and constant $C_B = 1$ when $P_B > 0$, and 0 otherwise. Whereas

$$f_1 = 1 + \left(\frac{0.05}{f_\mu}\right)^2 \tag{10}$$

$$f_2 = 1 - e^{-{R_T}^2} \tag{11}$$

$$f_\mu = \left[1 - e^{-0.025R_y}\right]^2 * \left(1 + \frac{20.5}{R_T}\right) \tag{12}$$

$$R_T = \frac{\rho k^2}{\mu\varepsilon} \tag{13}$$

$$R_y = \frac{\rho\sqrt{k}y}{\mu} \tag{14}$$

The values of constants C_μ, $C_{\varepsilon 1}$, $C_{\varepsilon 2}$, σ_k, σ_ε were set as:
C_μ=0.09, $C_{\varepsilon 1}$=1.44, $C_{\varepsilon 2}$=1.92, σ_k=1, σ_ε=1.3

SST k-ω equations

The Turbulence Kinetic Energy is written as

$$\frac{\partial k}{\partial t} + U_j\frac{\partial k}{\partial x_j} = P_k - \beta^*\omega k + \frac{\partial}{\partial x_j}\left((v + \sigma_k v_T)\frac{\partial k}{\partial x_j}\right) \tag{15}$$

The Specific Dissipation Rate is

$$\frac{\partial(p\omega)}{\partial t} + \frac{\partial(\rho u_j\omega)}{\partial x_j} = \alpha S^2 - \beta^*\omega^2 + \frac{\partial}{\partial x_j}\left((v + \sigma_\omega v_T)\frac{\partial \omega}{\partial x_j}\right) + 2(1 - F_1)\frac{\sigma_{w2}}{\omega}\frac{\partial k}{\partial x_i}\frac{\partial w}{\partial x_i} \tag{16}$$

where the terms are

$$F_1 = \tanh\{\{\min\left[\max\left(\frac{\sqrt{k}}{\beta^*\omega y}, \frac{500\nu}{y^2\omega}\right), \frac{4\sigma_{\omega 2}k}{CD_{k\omega}y^2}\right]\}^4\} \tag{17}$$

$$F_2 = \tanh\left[\left[\max\left(\frac{2\sqrt{k}}{\beta^*\omega y}, \frac{500\nu}{y^2\omega}\right)\right]^2\right] \tag{18}$$

$$P_k = \min\left(\tau_{ij}\frac{\partial U_i}{\partial x_j}, 10\beta^* k\omega\right) \tag{19}$$

$$\mathrm{CDk\omega} = \max\left(2\rho\sigma_{w2}\frac{1}{\omega}\frac{\partial k}{\partial x_i}\frac{\partial \omega}{\partial x_i}, 10^{-10}\right) \tag{20}$$

$$\phi = \phi_1 F_1 + \phi_2(1 - F_1) \tag{21}$$

And the constant coefficients are

$$\alpha_1 = \frac{5}{9},\ \alpha_2 = 0.44$$

$$\beta_1 = \frac{3}{40},\ \beta_2 = 0.0828$$

$$\beta^* = \frac{9}{100}$$

$$\sigma_{k1} = 0.85, \sigma_{k2} = 1$$

$$\sigma_{\omega 1} = 0.5, \sigma_{\omega 2} = 0.856$$

BSL Reynolds Stress Model

The Turbulent Kinetic Energy equation is

$$\frac{\partial(pw)}{\partial t} + \partial(Ukpw) = \frac{\alpha_3 w}{k}P_k + P_{wb} - \beta\ \ p\omega^2 + \frac{\partial}{\partial x_j}\left(\left(\mu + \mu\frac{t}{\sigma_{w3}}\ \ \right)\frac{\partial w}{\partial x_j}\right) + \frac{(1-F)2p1}{\sigma_{w3}}\frac{\partial k}{\partial x}\frac{\partial w}{\partial x} \tag{22}$$

The constant coefficients are

$$\alpha_2 = 0.44$$

$$\beta_2 = 0.0828$$

$$\beta^* = \frac{9}{100}$$

$$\sigma_1 = 1, \sigma_2 = 0.856$$

$$F_1 = \tanh\{\{\min\left[\max\left(\frac{\sqrt{k}}{\beta^*\omega y}, \frac{500\nu}{y^2\omega}\right), \frac{4pk}{CD_{k\omega\sigma_{k-e}}y^2}\right]\}^4\} \tag{23}$$

$$\mathrm{CDk\omega} = \max\left(2\rho\frac{1}{\omega}\frac{\partial k}{\partial x_i}\frac{\partial \omega}{\partial x_i}, 10^{-10}\right) \quad (24)$$

Reynolds stress Model equation are given below:

$$\frac{\partial}{\partial t}\left(\rho\overline{u_\iota u_j}\right) + \frac{\partial}{\partial x_k}\left(\rho u_k \overline{u_\iota' u_j'}\right) = -\frac{\partial}{\partial x_k}\left[\rho\overline{u_\iota' u_j' u_k'} + p'\left(\overline{\delta_{kj}u_\iota' + \delta_{\iota k}u_j'}\right)\right] + \frac{\partial}{\partial x_k}\left[\mu\frac{\partial}{\partial x_k}\left(\overline{u_\iota' u_j'}\right)\right] -$$
$$\rho\left(\overline{u_\iota' u_k'}\frac{\partial u_j}{\partial x_k} + \overline{u_j' u_k'}\frac{\partial u_i}{\partial x_k}\right) + \overline{p'\left(\frac{\partial u_\iota'}{\partial x_j} + \frac{\partial u_j'}{\partial x_\iota}\right)} - 2\mu\overline{\frac{\partial u_\iota'}{\partial x_k}\frac{\partial u_j'}{\partial x_k}} - 2\rho\Omega_k\left(\overline{u_j' u_m'}\epsilon_{ikm} + \overline{u_\iota' u_m'}\epsilon_{jkm}\right) \quad (25)$$

3. Numerical model setup

Ansys CFX was employed in the numerical simulations. The finite volume method with second-order accuracy was used to solve all the governing equations. The numerical calculations were conducted on the cube with 80x80x80 mm dimensions placed within the wind tunnel of 1120 mm in length and 320 mm in height. The mean inlet velocity at cube height was calculated from the Reynolds number of $4.6\text{x}10^4$, which resulted in 8.67 m/s. Air at 20º Celsius and 1 atm enters the wind tunnel through the inlet in the left and exists from the outlet as can be seen in Figure 1. Figure 1 also demonstrates the boundary conditions including inlet velocity and relative pressure.

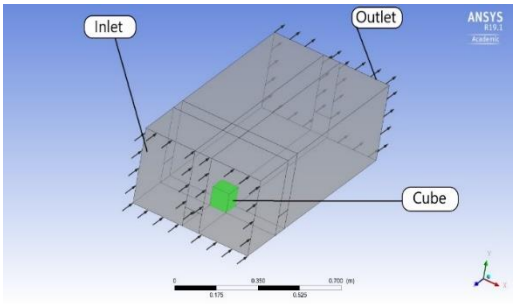

Figure 1. Boundaries and interfaces

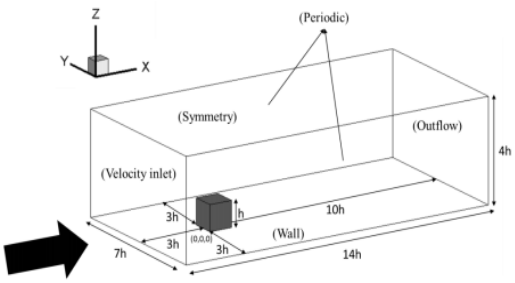

Figure 2. Computational domain and boundary conditions [11]

Figure 2 illustrates the experimental boundary conditions, the outflow (mass flow conservation for the outlet conditions) and symmetry conditions for the three-dimensional cube. Important setup specifications of the model are listed in Table 1.

Table 1. Setup specifications of the model [11]

Specification	Value
Distance from the inlet to the cube (left face)	240 mm
Distance from the cube to the outlet (right face)	800 mm
Cube height	80 mm

Inlet velocity	10 m/s
Outlet relative pressure	0 Pa
Reynolds number	46 000
Kinematic viscosity	$15x10^{-6}m^2/s$
Air density	$1.225\ g/m^3$

4. Mesh convergence study

The governing equations were discretized and solved using the finite volume method. Meshes were created using sweep meshing and inflation layers. The mesh convergence study was conducted using progressively denser meshes until the difference in the reattachment point of less than 1% was reached.

4.1. Y-plus

The y-plus value is a dimensionless distance from the wall. In turbulence modelling, it is an important parameter for Low Reynolds-Number (LRN) turbulence models [13]. Here the y-plus value was set below 3 in order to obtain accurate results in resolving the turbulent boundary layer. The initial mesh near to cube front face contained 700,012 nodes and 717,016 elements, and the y-plus value was around 7. Further mesh refinement was focused at the front face of the cube and the inflation method allowed to reduce the y-plus value from 7 to nearly 3. Finally, the elements size around the geometry were further reduced to reach the expected value. The final maximum y-value value was 1.4 at the front-edge of the cube. The resultant mesh contained 1,097,137 nodes and 1,031,610 elements. The result for y-plus is shown in Figure 3.

4.2. Mesh verification

Mesh verification analysis was conducted with 50% growth in the element number. As was mentioned earlier, less than 1% difference in reattachment point downstream of the cube was reached during the mesh verification process. Table 2 contains results of the mesh verification in several iterations with their errors and reattachment points.

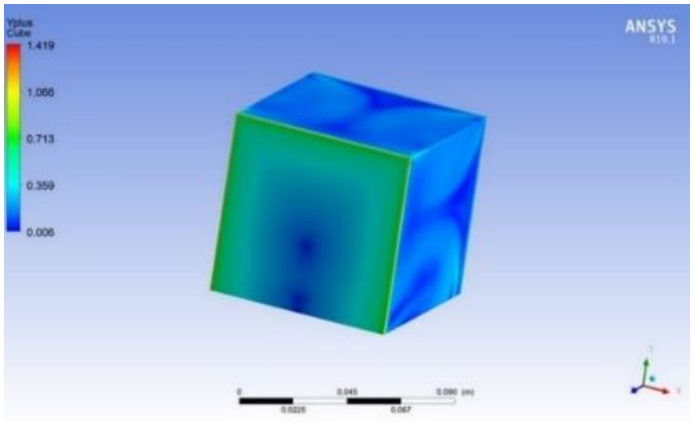

Figure 3. Y-plus along the cube surfaces

Table 2. Mesh verification

Iteration number	Reattachment points (m)	Error (%)	Elements	Nodes
1	1.84622	-	1,031,610	1,097,137
2	1.87646	1.61	2,470,177	2,588,366
3	1.89292	0.87	2,718,309	2,846,333
4	1.89471	0.09	3,309,530	3,453,597

From Table 2, it can be seen that the mesh convergence was achieved in the third iteration, when the relative error in the reattachment point was only 0.87%. Therefore, the mesh with 2,846,333 nodes and 2,718,309 elements was used for the further computational analysis. The resultant mesh around the cube is illustrated in Figure 4.

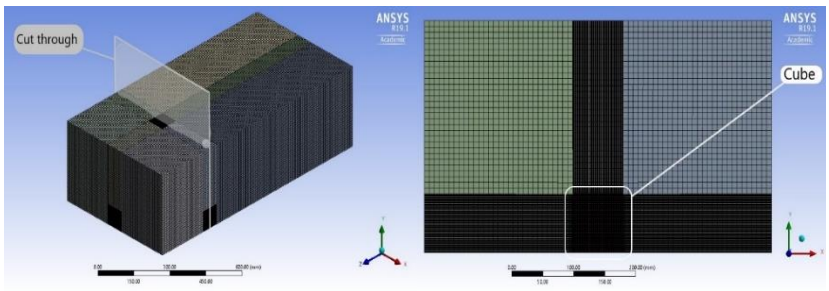

Figure 4. The resultant mesh and mesh density around the cube

5. Validation of the models

For the validation of the models, the experimental data and numerical results were compared. The comparison is done by using pressure coefficient values. To calculate the pressure coefficient the following definition was used:

$$C_p = \frac{P - P_r}{0.5 * \rho * U_h^2} \tag{26}$$

Where U_h is the free stream velocity and P_r is the mean static pressure upstream of the body. Obtained results were plotted in Figure 5, in which the horizontal axis represents the dimensionless length of the cube. The graph is divided in to three sections, which are 0-1, 1-2 and 2-3 and represent the front, top, and back sides of the cube, respectively. Figure 5 also shows the flow direction and the 0-1, 1-2, 2-3 flow paths.

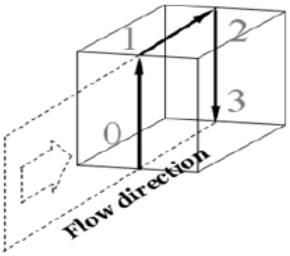

Figure 5. Flow over the central section of the cube [11]

The numerical results agree quite well for the front surface of the cube (0-1), where all the turbulence models show nearly the same results. According to the experimental data for the top surface of the cube, the pressure first decreases after the separation point and increases through the left length. However, as the flow reaches the top surface significant deviations between numerical and experimental results occur. As can be observed in Figure 6, the k-ω model has the least accurate data for the top surface. The k-ε model is more accurate than k-ω, but still has a noticeable difference. The SST model shows a more accurate trend, but the BSL Reynolds model shows the best numerical results for 1-2 region. According to empirical data, the pressure distribution on the back side of the cube should remain constant with slight increase in the pressure coefficient. For this region The BSL Reynolds model shows similar behaviour for the beginning of the region 2-3 but starts deviating towards the end. The k-ε and k-ω models show a similar trend, but the k-ε model's values were higher than the experimental data, while k-ω produced lower values. The SST model results lie between k-ε and k-ω and are closer to the experimental data than the other models. Here the SST model shows better performance because the model uses the combination of the k-ε and k-ω models. Overall, for the

back side of the cube all the models show certain deviation, which might be due to the complex fluid flow that includes vortices, separation, and reattachment of the flow, and the viscosity effects. To sum up, for the 3-D case the BSL Reynolds and SST models show accurate results in comparison with the k-ε and k-ω models.

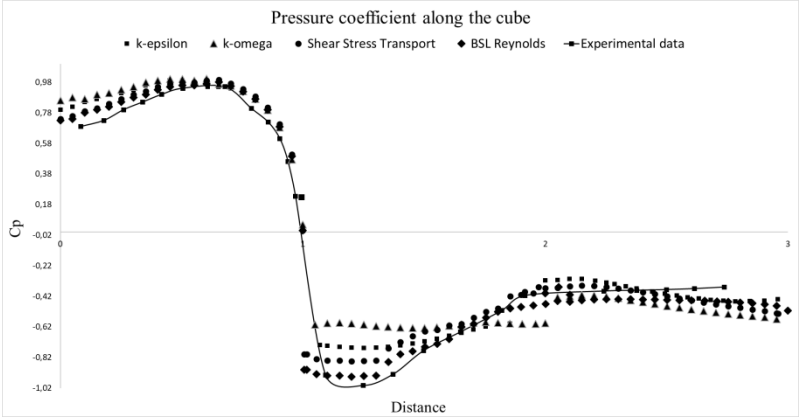

Figure 6. Pressure distribution along the cube surface

The 2-D case of the flow around the cube was also studied in this work. The numerical results for the 2-D case were generated using the same boundary conditions and dimensions and were compared with the 3-D case. Figure 7 shows the comparison, in which the surface pressure distribution is also divided into three sections that are the front, top, and back side of the cube. For the front side the 3-D numerical analysis show more accurate results, while the 2-D numerical values remained constant along the distance. Moreover, at the top surface, the results deviate nearly by factor of 3. The back side of the cube also shows large variations. Overall, the trends of the curves for both cases are similar, but the actual values differ considerably. The reason is that in the 2-D case the air flows in one direction only – along the top surface of the cube, while in the 3-D case the flow also tends to travel around the sides of the cube as shown in Figure . According to [14] for the 3-D finite shaped geometries, the flow will be developed steadily over all sides and Bernoulli's equation can be used to determine the pressure. However, in the 2-D case at the top surface flow separation starts suddenly and the flow recirculation in the wake region is much stronger, where viscous effects become more significant, thus resulting in very steep decrease and increase in pressure and much lower pressure level there than the 3D case.

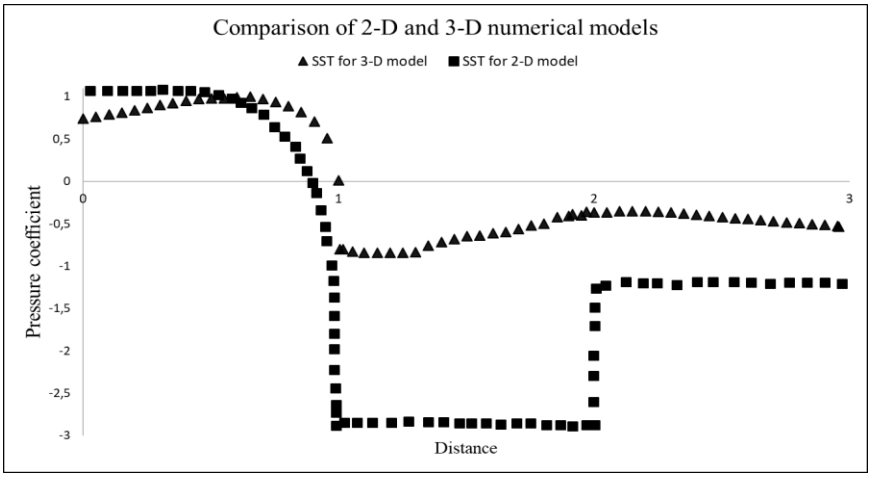

Figure 7. Pressure coefficient around the 2-D and 3-D cubes

Finally, according to the obtained numerical results, the SST and BSL Reynolds models can predict the flow more accurately than the others, but in general, the BSL Reynolds model has the least

discrepancy. Here the pressure and velocity contours, and streamlines have been plotted for this model (Figures 8-9). Figure (a) and (b) show the pressure and velocity contours around the cube from the top. There is stagnation at the front surface of the cube, where pressure increases but velocity approaches zero. Moreover, Figure (b) shows flow separation around the sides of the cube and formation of the wake region. The vortices formed in the wake region can be observed in Figure . From the streamlines, it can be noticed that after the stagnation point the fluid starts accelerating, which causes recirculation of the flow and creation of vortices. A clearer view of the recirculating flow is shown from the bottom side of the cube in Figure 8.

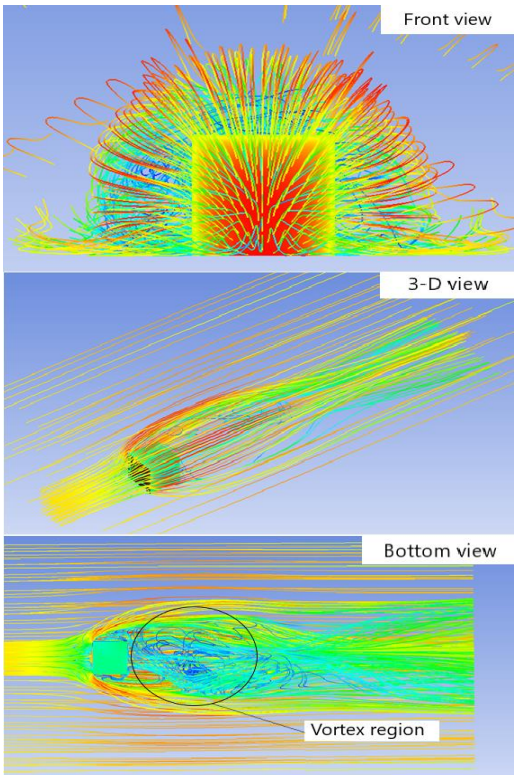

Figure 8. Streamlines of the flow around the cube in the 3D simulations

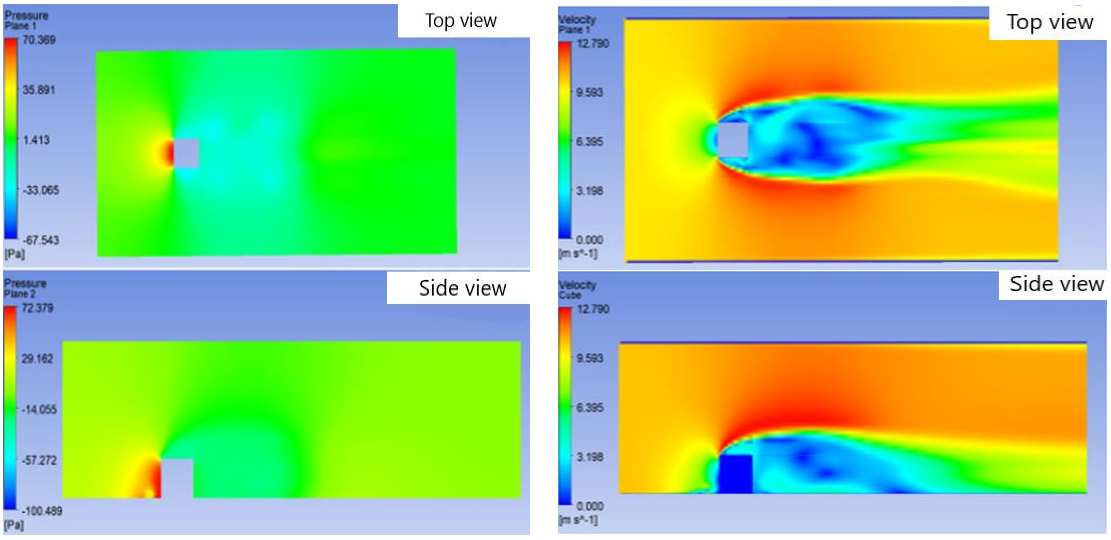

Figure 9. (a) pressure contours | (b) velocity contours

6. Conclusion

Numerical simulations were performed on the turbulent flow around 3-D cube geometry by using the Ansys CFX software. The main aim of the study was to compare four turbulence models, namely k-ε, k-ω, SST, and RSM models and to identify the most efficient turbulence model that accurately describes the flow around the cube. During the investigation, the values of the pressure coefficient (Cp) on the front, top, and back sides of the cube were obtained and compared with experimental data.

Numerical analysis demonstrates that the SST and RSM turbulent models produce more accurate results for separated flows with circulating vortices, than the k-ε and k-ω models. Furthermore, the RSM has less deviation from the empirical data than the SST model. However, it necessary to consider the fact that the RSM needs to solve seven equations, while SST solves only two, which affects the cost of the computations. Therefore, if there is not enough computational power available, SST model can be used instead of the RSM. For the 2-D and 3-D cases the pressure coefficient values were quite different. It was because the actual flow is fully 3D and turbulent with flow separations around the cube.

References

[1] Heidarzadeh, H., Farhadi, M., & Sedighi, K. (2012). Convective heat transfer over a wall mounted cube using large eddy simulation. CFD Letters, 4(2), 80-92.
[2] Lim, H. C., Thomas, T. G., & Castro, I. P. (2009). Flow around a cube in a turbulent boundary layer: LES and experiment. Journal of Wind Engineering and Industrial Aerodynamics, 97(2), 96-109.
[3] Lim., H. C., Castro, I.P., (2006). Turbulent Boundary Layer Flow Over a Cube. European Research Community on Flow, Turbulence and Combustion, Ercoftact databases. Main page.
[4] Kiislicina, Yu. (2018, January 11). High speed hurricane damaged buildings including Universities in Astana. Radio Sputnik, Retrieved from https://ria.ru/world/20180111/1512424874.html
[5] Oliver, K. (2018, March 5). Wind statics for Astana including 2018 year. Windfinde, Retrieved from https://www.windfinder.com/windstatistics/astana
[6] Zhumanova, D. (2018, January 11). Critical weather condition after strong hurricane. Commercial television channel KTK, Retrieved from https://www.ktk.kz/ru/news/video/2018/01/11/87774
[7] Köppen, B. (2013). The production of a new Eurasian capital on the Kazakh steppe: architecture, urban design, and identity in Astana. Nationalities Papers, 41(4), 590-605.
[8] Abohela, I., Hamza, N., & Dudek, S. (2013). Effect of roof shape, wind direction, building height and urban configuration on the energy yield and positioning of roof mounted wind turbines. Renewable Energy, 50, 1106-1118.
[9] Castro, I.P. & Robins, A.G. (1977). The flow around a surface mounted cube in uniform and turbulent streams. J. Fluid Mech., 79, 307-355.
[10] Murakami, S., & Mochida, A. (1995). On turbulent vortex shedding flow past 2D square cylinder predicted by CFD. Journal of Wind Engineering and Industrial Aerodynamics, 54, 191-211.
[11] Lee, Y. T., Boo, S. I., Lim, H. C., & Misutani, K. (2016). Pressure distribution on rectangular buildings with changes in aspect ratio and wind direction. Wind and Structures, 23(5), 465-483.
[12] Fimbres-Weihs, G. A., & Wiley, D. E. (2010). Review of 3D CFD modeling of flow and mass transfer in narrow spacer-filled channels in membrane modules. Chemical Engineering and Processing: Process Intensification, 49(7), 759-781.
[13] Ariff, M., Salim, S. M., & Cheah, S. C. (2009, December). Wall y+ approach for dealing with turbulent flow over a surface mounted cube: Part 1—Low Reynolds number. In Seventh International Conference on CFD in the Minerals and Process Industries (pp. 1-6).
[14] Gao, Y. and Chow, W.K., 2005. Numerical studies on air flow around a cube. Journal of Wind Engineering and Industrial Aerodynamics, 93(2), pp.115-135.